https://doi.org/10.32604/zkg.2026.080546

ARTICLE

Evolution and mechanism of high-temperature performance of magnesium ammonium phosphate cement

Yi Liu[1,#], Jinguang Zhao[1,#], Pengkun Hou[1,*], Hongsheng Wang[2,*], Shuang Liang[3,*] and Jie Hu[4]
[1]School of Materials Science & Engineering, University of Jinan, Jinan, China
[2]Shandong Industrial Ceramic Research & Degisn Insitute Co., Ltd., Zibo, China
[3]School of Civil Engineering, University of Leeds, Leeds, UK
[4]School of Materials Science and Engineering, South China University of Technology, Guangzhou, China
*Corresponding Authors: Pengkun Hou. Email: pkhou@163.com; Hongsheng Wang. Email: wanghs721@126.com; Shuang Liang. Email: s.liang@leeds.ac.uk
[#]Co-First Author: Yi Liu and Jinguang Zhao

Received: 11 February 2026; Accepted: 16 March 2026

ABSTRACT: Although magnesium ammonium phosphate cement exhibits promising thermal resistance, the effects of mix proportions on its phase evolution and performance at high temperatures remain unclear. This study investigated the effects of magnesia-to-phosphate, water-to-cement, and boric acid to-magnesia ratios on the performance of magnesium ammonium phosphate cement (MAPC) after exposure to temperatures up to 1000°C. Some engineering properties and residual strength were tested and phase evolution was revealed using X-ray diffraction (XRD) and scanning electron microscopy (SEM). Results indicated that boric acid-to-magnesia ratio (B/M) most strongly controlled high-temperature degradation. Although a lower B/M ratio reduced strength at room temperature (20°C), it enhanced exposure to high temperatures residual strength by mitigating boric acid dehydration and adverse phase transformations. Notably, MAPC specimens with 5–10% boric acid achieved an optimal residual strength of 19.9 MPa at 1000°C. In addition, increasing the magnesia-to-phosphate ratio (M/P) and decreasing the water-to-cement ratio (W/C) improved high-temperature strength and reduced porosity by ensuring sufficient residual MgO. At 1000°C, increasing the M/P ratio from 1.5 to 3.0 elevated the residual compressive strength from 4.8 MPa to 7.8 MPa, while concurrently reducing the porosity from 42.80% to 41.38%. Reducing the W/C ratio from 0.20 to 0.15 bolstered the residual compressive strength from 7.8 MPa to 9.2 MPa, while simultaneously decreasing the porosity from 41.38% to 30.20%. $MgNH_4PO_4{\cdot}6H_2O$ transformed into $Mg_3(PO_4)_2$ after exposure to 800°C. However, with 20% boric acid, the reaction between $Mg_3(PO_4)_2$, MgO, and B_2O_3 formed plate-like $Mg_3(BO_3)(PO_4)$ clusters at 1000°C. The associated mass loss and inter-layer microcracks were identified as the primary causes of strength reduction. This study systematically investigates the influence of M/P, W/C, and B/M ratios on the high-temperature performance of MAPC, with a focus on the mechanisms underlying the substantial impact of the B/M ratio.

KEYWORDS: Magnesium ammonium phosphate cement; magnesia-to-phosphate ratio; boric acid-to-magnesia ratio; water-to-cement ratio; high-temperature resistance

MATERIALS

1 Introduction

Building fires are characterized by their sudden onset and rapid heating rates, which induce internal thermal stresses in cement-based materials, leading to cracking, strength degradation, and the risk of explosive spalling [1]. In ordinary Portland cement (OPC) systems dominated by calcium silicate hydrate (C-S-H) gel, dehydration and the decomposition of the gel structure at high temperatures result in rapid structural deterioration [2]. To meet the requirements for structural fire resistance, developing materials capable of maintaining structural integrity and performance stability at high temperatures is crucial for enhancing fire safety capabilities. Magnesium ammonium phosphate cement (MAPC) is an inorganic cementitious material formed via an acid-base reaction between magnesia (MgO) and ammonium dihydrogen phosphate ($NH_4H_2PO_4$) under the regulation of retarders (e.g., borax or boric acid), with struvite ($MgNH_4PO_4{\cdot}6H_2O$) as the primary phase. Due to its rapid setting [3, 4] and high early strength [5–8], high bonding strength [9], and low drying shrinkage [10, 11], MAPC has been widely applied in fields such as the rapid repair of concrete structures [12, 13] and the immobilization of radionuclides [14]. Zhang [15] reported that the residual compressive strength of MAPC after exposure to 1000°C was 18.0 MPa higher

than that of ordinary Portland cement (23.7 MPa vs. 5.0 MPa). Consequently, the high-temperature resistance of MAPC has attracted extensive attention in recent years [16–20].

A series of studies have been conducted on the performance evolution of MAPC at high temperatures [21, 22]. Bhuiyan et al. [23] reported the stepwise dehydration of struvite (105–200°C) and the release of ammonia (200–600°C) in MAPC at elevated temperatures, which could induce porosity growth and crack evolution. Subsequently, the resulting thermally stable phases 20 may form a load-bearing skeleton together with residual MgO [24], thereby determining the residual strength. Hipedinger et al. [25] reported that magnesium phosphate cement (MPC) retained flexural strength of 14.0 MPa after exposure to 1350°C (heating rate of 5°C/min, holding time of 2 h). Sugama and Kukacka [26] reported that when MPC were heated to 1300°C, the material underwent a phase transformation to form anhydrous magnesium phosphate ($Mg_3(PO_4)_2$), increasing the compressive strength to 48.2 MPa.

In terms of enhancing the high-temperature stability of MAPC, current research has largely focused on optimizing the pore structure and thermal properties through the incorporation of mineral admixtures and functional fillers [27–29]. Liu et al. [30] reported that silica fume enhanced the residual mechanical properties of MPC by pore filling, increasing residual compressive strength at 800°C from 10.0 MPa to 19.0 MPa. Dai et al. [31] reported that α-Al_2O_3 significantly improved the volumetric stability of MPC at high temperatures. With an α-Al_2O_3 dosage of 80%, the shrinkage rate was only –0.9% (indicating slight expansion) after exposure to 1300°C. Yu et al. [32] reported that MPC incorporated with 10% sulphoaluminate cement retained a compressive strength of approximately 56.0 MPa after exposure to 1100°C. This improvement was attributed to the pore-filling effect of the sulphoaluminate cement and the promotion of liquid-phase sintering at high temperatures. However, existing studies have primarily focused on modification measures. While the high-temperature residual performance of MAPC is governed by phase reorganization and structural deterioration, a systematic elucidation of the phase transformation and pore evolution characteristics regulated by the mix proportions (M/P, W/C, and B/M) is still lacking.

The mix proportion of MAPC dictates the type and content of initial hydration phases (e.g., struvite, other hydrates and residual MgO), which directly influences the phase transformation and pore structure at high temperatures, thereby constituting a fundamental variable affecting its high-temperature service performance [33, 34]. You [3] reported that the M/P, W/C, and B/M ratios are critical factors governing the room-temperature performance of MAPC. In recent years, although extensive research has been conducted on the high-temperature performance of MAPC, reports concerning the effect of the W/C ratio remain relatively scarce. In particular, a systematic investigation into the impact of three critical parameters (M/P, W/C, and B/M ratios) on its high-temperature properties is still lacking. Although existing studies have laid a foundation for understanding the phase evolution and macroscopic property changes of MAPC, a systematic and quantitative understanding of how these mix proportions (M/P, W/C, and B/M) influence the phase composition and structural evolution after high-temperature exposure remains lacking.

This study comprehensively investigates the effects of mix proportions on the residual performance of MAPC pastes after high-temperature exposure. Typical MAPC formulations were prepared with M/P ratios of 1.5, 2.0, and 3.0; W/C ratios of 0.15, 0.18, and 0.20; and B/M ratios of 5%, 10%, and 20%. Residual compressive strength, mass loss, and porosity was systematically evaluated after exposure to 600°C, 800°C, and 1000°C. Furthermore, X-ray diffraction (XRD) and scanning electron microscopy (SEM) were employed to characterize the phase transitions and microstructural evolution of the pastes after high-temperature exposure. This study aims to systematically research the effects of M/P, W/C, and B/M ratios on the high-temperature performance of MAPC, providing a theoretical basis for enhancing its fire resistance. The mechanisms underlying the significant influence of the B/M ratio are specifically elucidated through XRD and SEM analyses.

2 Materials and methods

2.1 Raw materials

The dead-burnt magnesia (M) used in this study was sourced from Anshan, Liaoning Province, China, with a specific surface area of 245 m^2/kg. Industrial-grade ammonium dihydrogen phosphate (P, purity > 98%) and boric acid (B, purity > 95%) were employed as the phosphate source and retarder, respectively. The chemical compositions of magnesium oxide and ammonium dihydrogen phosphate determined by XRF are summarized in Table 1. The XRD pattern and particle

Table 1 Chemical composition of the magnesia

Material	Chemical Composition (wt.%)								
	MgO	SiO_2	CaO	Fe_2O_3	Al_2O_3	P_2O_5	SO_3	MnO	Other
M	90.81	3.49	1.71	1.70	1.18	0.67	0.21	0.14	0.09
P	—	0.20	—	—	—	66.28	1.85	—	0.57

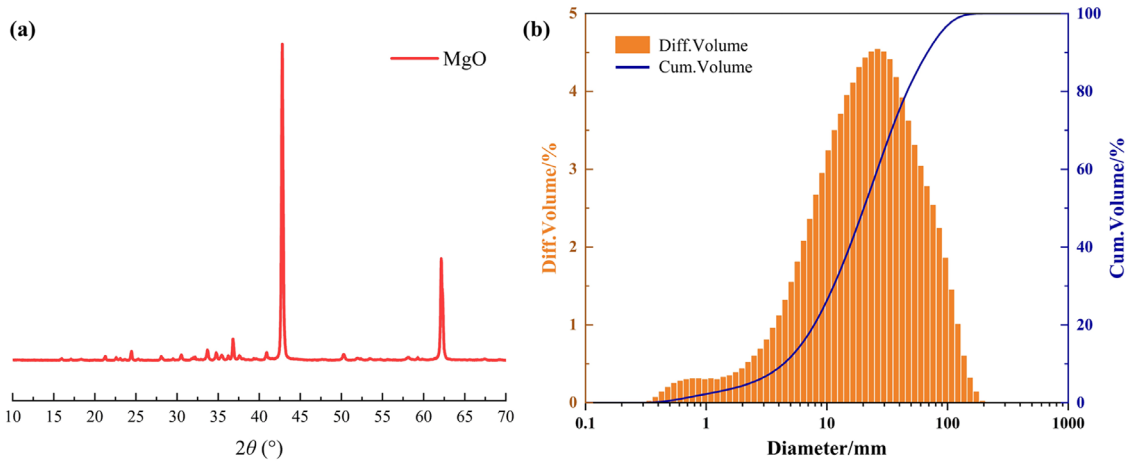

Figure 1 XRD (a) and particle size distribution (b) of the magnesia

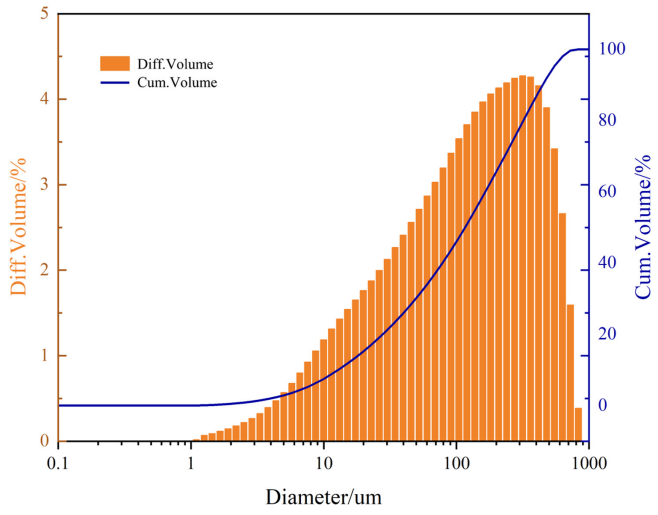

Figure 2 Particle size distribution of the ammonium dihydrogen phosphate

size distribution of M are presented in Figure 1, and the particle size distribution of P is shown in Figure 2. XRF analysis determined the total content of heavy elements in P to be 68.90%.

2.2 Mix proportion and sample preparation

The MAPC pastes were prepared with M/P of 1.5, 2.0, and 3.0, W/C of 0.15, 0.18, and 0.20, B/M of 5%, 10%, and 20%. The mix proportions in this study were centered on the M/P = 2.0 and W/C = 0.20 ratios commonly reported in literature, within a certain range of M/P and W/C ratios selected for investigation. The detailed mix proportions are listed in Table 2.

The raw materials were weighed according to the specified mix proportions and placed into a mortar mixer. The mixture was first dry-mixed at low speed for 1 min, followed by wet mixing for 3 min. Subsequently, the resulting paste was cast into 40 mm × 40 mm × 40 mm plastic molds. The pastes were cured indoors (20 ± 1°C, RH > 90 ± 2%) for 5 h before being demolded. They were

Table 2 Mix proportions of the experiments

Mixture	Mix proportions (wt.%)			M/P	W/C	B/M
	MgO	$NH_4H_2PO_4$	H_3BO_3			
1	53.6	35.7	10.7	1.5	0.20	20%
2	58.8	29.4	11.8	2.0	0.20	20%
3	65.2	21.7	13.1	3.0	0.20	20%
4	65.2	21.7	13.1	3.0	0.15	20%
5	65.2	21.7	13.1	3.0	0.18	20%
6	72.3	24.1	3.6	3.0	0.15	5%
7	69.7	23.3	7.0	3.0	0.15	10%

then returned to the same environment for further curing. High-temperature performance tests were conducted on the pastes after 1 d, 7 d, and 28 d.

2.3 Testing methods

2.3.1 High-temperature testing regime

The high-temperature performance of MAPC was evaluated after exposure to 600°C, 800°C, and 1000°C. Upon reaching the specified curing ages, the pastes were heated in a muffle furnace (Model SXL-1700C, Shanghai Jujing Precision Instrument Manufacturing Co., Ltd.). Once the furnace reached the target temperature, pastes were placed inside and held for 30 min. The heating rate of the muffle furnace was set to 10°C/min. Once the furnace reached the target experimental temperature and stabilized, the cured specimens were directly placed inside for heat treatment. Upon completion of the heating process, the specimens were immediately removed and allowed to cool in air to room temperature prior to performance testing.

2.3.2 Setting time

The setting time test was conducted in accordance with the Chinese National Standard GB/T 1346-2024 (*Test methods for water requirement of normal consistency, setting time and soundness of cement*). The setting time of the MAPC pastes was determined using a Vicat apparatus, with the zero-time point defined as the moment when water was added to the mixture.

2.3.3 Porosity

The open porosity of the MAPC was determined by the Archimedes method and calculated according to Equation (1):

$$P = \frac{m_W - m_D}{m_W - m_a} \times 100\% \quad (1)$$

where m_D, m_W, and m_a are the mass of the dried paste, the water-saturated paste, and the paste suspended mass in water, respectively. All masses were determined with a precision of 0.01 g. Specimens with dimensions of 40 * 40 * 40 mm³ were prepared and cured for 1, 7, and 28 days, respectively. The reported mass porosity is the average value obtained from three pastes.

2.3.4 Compressive strength

The compressive strength of the MAPC pastes was determined in accordance with GB/T 17671 2021 (*Test Method for Strength of Cement Mortar (ISO Method)*). A combined compression and flexural testing machine (Model CDT 1305-2, METS Industrial Systems Co. Ltd.) was used to test the pastes before and after high-temperature exposure. Specimens with dimensions of 40 * 40 * 40 mm³ were prepared and cured for 1, 7, and 28 days, respectively. The reported mass porosity is the average value obtained from three pastes. The reported compressive strength is the average value obtained from six pastes.

2.3.5 Mass loss

The mass loss of the MAPC was calculated from the paste mass before (m_1) and after (m_2) the high-temperature test, as shown in Equation (2). All masses were measured with a precision of 0.01 g. Specimens with dimensions of 40 * 40 * 40 mm³ were prepared and cured for 1, 7, and 28 days, respectively. The reported mass porosity is the average value obtained from three pastes. The reported mass loss is the average value obtained from three pastes.

$$\Delta m = \frac{m_1 - m_2}{m_1} \times 100\% \quad (2)$$

2.3.6 Mineralogical evolutions

For hydration termination, the MAPC pastes, after the high-temperature test, were crushed and immersed in isopropanol (purity ≥ 99.5%), which was replaced twice at 24-h intervals. The samples were then dried at 40°C for 48 h, ground, and sieved through a 200-mesh sieve. For analysis, the MAPC pastes were ground to pass a 200-mesh sieve after high-temperature exposure.

For quantitative phase analysis, 20 wt.% of α-Al_2O_3 was incorporated into the powder samples as an internal standard. The mixture was then wet-ground with anhydrous ethanol, dried, and collected. The phase composition was analyzed using an XRD (D8-Advance, Bruker, Germany). The instrument was equipped with a Cu anode (λ = 1.54184 Å) and operated at 40 kV and 40 mA. Data were collected over a 2θ range of 5° to 80° with a scan rate of 2° (2θ)/min and a step size of 0.02°. Quantitative analysis was performed using the Rietveld method implemented in Topas software.

2.3.7 SEM

The SEM micrograph of the MAPC pastes was observed using a JSM-7610F field-emission scanning electron microscope (SEM, JEOL, Japan), which was equipped with an energy-dispersive spectrometer (EDS) for elemental composition analysis. Prior to examination, the bulk pastes were sputter-coated with gold for 60 s. The analysis was conducted at an accelerating voltage of 10 kV.

3 Results and discussion

3.1 Setting time and fluidity

Figure 3 shows the effects of M/P, W/C, and B/M ratios on the setting time and fluidity of MAPC pastes. It can be observed that both the setting time and fluidity decrease with an increasing M/P ratio. As shown in Figure 3a, when the M/P ratio increases from 1.5 to 3.0, the setting time shortens from 15.5 min to 12.0 min, and the fluidity decreases from 235 mm to 215 mm. This

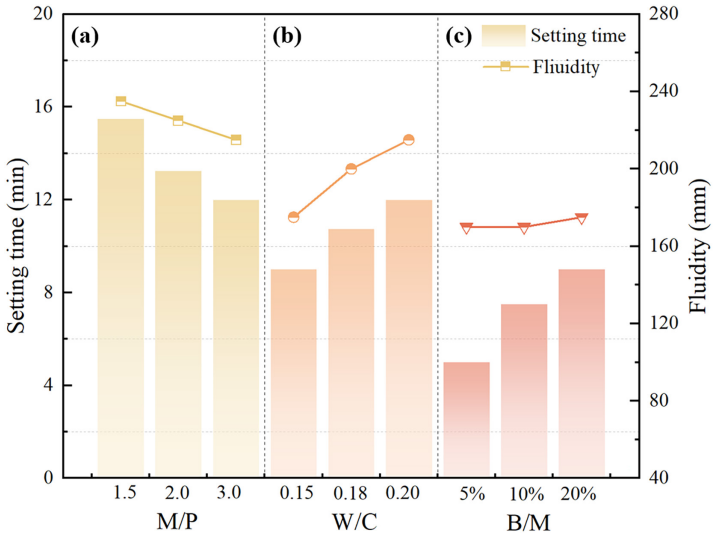

Figure 3 Effects of M/P (a), W/C (b), and B/M (c) ratios on the setting time and fluidity of MAPC pastes

phenomenon may be attributed to the increased relative content of MgO in the system at higher M/P ratios. The resulting higher concentration of Mg^{2+} at the early hydration stage facilitates the formation of phosphate hydration products, thereby promoting rapid crystal nucleation and subsequent interlocking, which shortens the setting time [35]. Simultaneously, increasing the MgO content raises the water demand and promotes particle flocculation [36–38].

Conversely, both the setting time and fluidity of the MAPC pastes increase with an increasing W/C ratio. As shown in Figure 3b, when the W/C ratio is raised from 0.15 to 0.20, the setting time is prolonged from 9.0 min to 12.0 min, and the fluidity improves from 175 mm to 215 mm. Increasing the water content dilutes the concentration of reactive ions (e.g., Mg^{2+} and PO_4^{3-}) in the pore solution, thereby reducing the degree of supersaturation and the nucleation rate [39]. This retards the formation of hydration products, consequently prolonging the setting time.

Both the setting time and fluidity of the MAPC pastes increase with an increasing B/M ratio. As shown in Figure 3c, with the B/M ratio increasing from 5% to 20%, the setting time increases from 5.0 min to 9.0 min, while the fluidity increases slightly from 170 mm to 175 mm. This behavior is attributed to the increased complexation of Mg^{2+} at higher boric acid dosages, which inhibits the early dissolution of MgO [40] and the nucleation and growth of hydration products [41], thereby leading to a prolonged setting time.

3.2 Compressive strength

Figure 4 shows the influence of the M/P ratio on the compressive strength of MAPC pastes at 1 d, 7 d, and 28 d, before and after high-temperature exposure. The compressive strength of all groups decreases continuously as the exposure temperature increases from 20°C to 1000°C. As shown in Figure 3a, the compressive strength of the paste with M/P = 3.0 decreases from 17.8 MPa at 20°C to approximately 5.2 MPa at 1000°C. This reduction is primarily ascribed to the dehydration and decomposition of hydration products (e.g., struvite) during high-temperature exposure, which generates numerous pores and microcracks, thereby compromising the load-bearing capacity of the pastes [15]. Zhang [15] also report that the thermal decomposition of hydration products is one of the critical factors impairing the high-temperature performance of MPC.

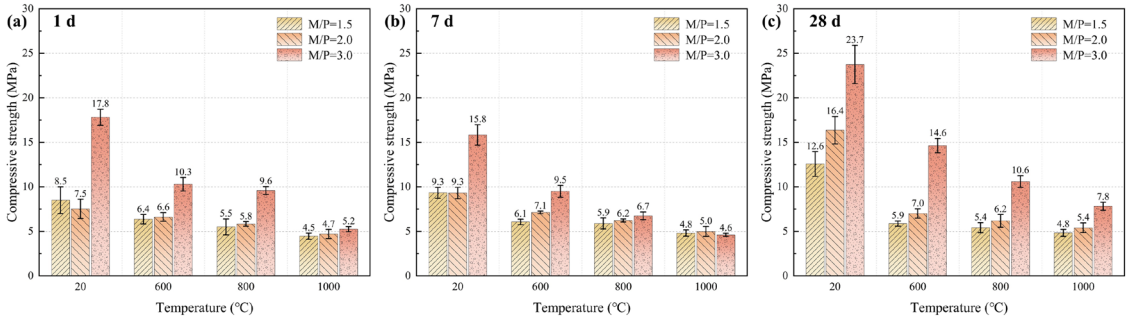

Figure 4 Effect of the M/P ratio on the compressive strength of MAPC pastes before and after high-temperature exposure (W/C = 0.20, B/M = 20%, (a): 1 d, (b): 7 d, (c): 28 d)

It is worth noting that at the same high-temperature exposure, MAPC pastes with higher M/P ratios exhibit higher residual compressive strength. For instance, at the curing age of 28 d (Figure 4c), after exposure to 1000°C, the compressive strength of the paste with M/P = 3.0 reaches 7.5 MPa, which is significantly higher than that of the M/P = 1.5 and 2.0 groups (5.4 MPa). This improvement may be attributed to the formation of a continuous skeletal structure dominated by excess MgO and anhydrous phosphates at high temperatures. Additionally, a sintering-controlled densification occurs during the heating process, thereby enhancing the residual compressive strength.

With increasing curing age, the residual compressive strength of the MAPC pastes after high-temperature exposure also exhibits an increasing trend. Comparing Figure 4b with Figure 4c, it can be observed that for the condition of M/P = 3.0, the residual compressive strength after exposure to 1000°C increases from approximately 4.6 MPa at 7 d to approximately 7.8 MPa at 28 d, representing an increase of about 69.6%. This improvement is primarily attributed to the more complete hydration reaction at 20°C temperature over a longer curing period. This is primarily attributed to the more complete hydration at ambient temperature over a prolonged curing period. The continuous formation of hydration products fills the capillary pores, thereby densifying the matrix structure and forming a more continuous load-bearing skeleton.

The continuous formation of primary hydration products fills the capillary pores, further densifying the matrix structure and forming a relatively continuous load-bearing skeleton. Although the dehydration and decomposition of hydration products are inevitable during high-temperature exposure, the dense skeleton formed at the early stage, along with certain thermally stable phases, is retained, thereby ensuring a higher residual compressive strength.

Figure 5 shows the influence of the W/C ratio on the compressive strength of MAPC pastes at 1 d, 7 d, and 28 d, before and after high-temperature exposure. The residual compressive strength of all groups gradually decreases with increasing exposure temperature (consistent with the findings for the M/P ratio). At 7 d and 28 d, pastes with a lower W/C ratio exhibit higher residual compressive strength. For instance, at 28 d (Figure 5c), the paste with W/C = 0.15 exhibits a residual compressive strength of 19.2 MPa after exposure to 800°C, which is significantly higher than that of W/C = 0.18 (14.2 MPa) and W/C = 0.20 (10.6 MPa). This phenomenon is likely associated with the reduced free water content and denser capillary pore structure resulting from a lower W/C ratio. Such a microstructure minimizes pore coarsening and thermally induced microcracking caused by moisture migration and dehydration during heating, thereby enhancing the residual compressive strength [30]. However, at 1 d, the strength of the W/C = 0.18 group is notably higher, suggesting the existence of an optimal range of mixing water content for the early-stage hydration reaction.

Consistent with the trends discussed in the previous section, increasing curing age generally enhanced the residual compressive strength after high-temperature exposure, due to more complete hydration and a denser pre-formed matrix. As shown in Figure 5a,5c, the residual compressive strength of the paste with W/C = 0.15 after exposure to 800°C increases from 10.7 MPa at 1 d to 19.2 MPa at 28 d. It is observed that when the exposure temperature rises to 1000°C, the difference in residual compressive strength among different W/C ratios diminishes. As shown in Figure 5c, the residual compressive strengths of the three groups after exposure to 1000°C are 9.2 MPa, 9.2 MPa, and 7.8 MPa, respectively, with a difference of less than 2 MPa. For comparison, the difference between W/C = 0.15 and 0.20 was approximately 6.0 MPa after exposure to 600°C (20.6 MPa vs. 14.6 MPa) and approximately 8.6 MPa after exposure to 800°C (19.2 MPa vs. 10.6 MPa). This indicates that at 1000°C, the residual compressive strength of the system is more likely dominated by the skeleton formed by MgO and $Mg_3(PO_4)_2$ [32]. The differences in initial pore structure and hydration product distribution caused by the W/C ratio at early stages are

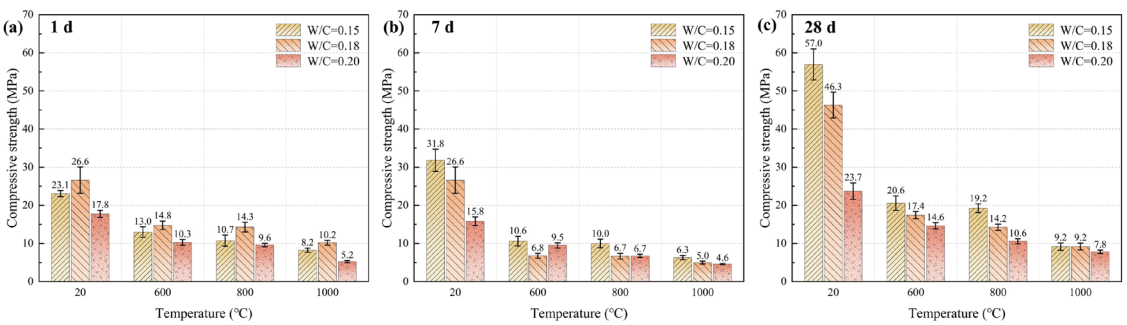

Figure 5 **Effect of the W/C ratio on the compressive strength of MAPC pastes before and after high-temperature exposure (M/P = 3.0, B/M = 20%, (a): 1 d, (b): 7 d, (c): 28 d)**

attenuated during the high-temperature dehydration, decomposition, and structural reconstruction, resulting in a convergence of the residual compressive strength.

Figure 6 shows the effects of the B/M ratio on the compressive strength of MAPC pastes at 1 d, 7 d, and 28 d, before and after high-temperature exposure. It can be observed that at 20°C temperature, the compressive strength increases with an increasing B/M ratio (B/M = 5%_30.8 MPa, B/M = 10%_49.3 MPa, B/M = 20%_57.0 MPa). This phenomenon may be attributed to the fact that a high boric acid dosage regulates the early reaction kinetics of MAPC, prolonging the setting time. This facilitates the filling of pores by hydration products, thereby forming a more compact structure. Hall et al. [40] also report that high boric acid content can indirectly alter the microstructure by regulating the setting and hardening process, as well as crystal nucleation and growth modes, ultimately leading to strength enhancement.

Although boric acid can enhance the strength of MAPC at 20°C temperature, an excessive dosage leads to lower residual compressive strength after high-temperature exposure, which is particularly pronounced at 1000°C. For instance, at 7 d (Figure 5b), the residual compressive strengths of MAPC pastes after exposure to 1000°C are 18.1 MPa (B/M = 5%) and 17.4 MPa (B/M = 10%), whereas that of the B/M = 20% group plummets to 6.3 MPa. This may be attributed to the fact that excess boric acid is more prone to undergoing dehydration and transformation into borates during heating, forming boron-rich glass phases or low-melting phases. A possible mechanism for this behavior is that the process is accompanied by increased mass loss and pore growth. Concurrently, the softening of low-melting phases and thermal expansion mismatches may induce further thermal microcracking. These factors could weaken the continuity of the sintered skeleton formed jointly by MgO and high-temperature phosphate phases [42], potentially leading to a significant reduction in residual strength.

Notably, the pastes with B/M = 5–10% exhibit stable residual compressive strength (16.8–23.7 MPa) after exposure to temperatures in the range of 600–1000°C. This behavior can be attributed to an optimal balance between retardation and densification achieved at moderate boric acid additions (5–10 wt.%). Such dosages are sufficient to mitigate the defects associated with an excessively rapid initial reaction, yet are low enough to avoid the exacerbated high-temperature damage observed at higher dosages. Consequently, a more stable residual compressive strength is maintained over the 600–1000°C temperature range. For the B/M = 20% group, the residual compressive strength after high-temperature exposure initially decreases and subsequently increases with extending curing age. At 600°C, the residual compressive strength decreases from 13.0 MPa at 1 d to 10.6 MPa at 7 d, and then rises to 20.6 MPa at 28 d. This phenomenon may be ascribed to the coexistence of substantial hydrous hydration products and unreacted phases in the high-boron system at the intermediate stage (about 7 d), where dehydration decomposition and internal vapor pressure during heating are more prone to inducing structural damage. Extending the curing period to 28 d ensures more complete hydration, further pore filling, and stable phase composition, which facilitates sintering reconstruction at high temperatures, thereby enhancing the residual compressive strength.

3.3 Mass loss

The mass loss behavior of MAPC during the heating process can be characterized as a multi-stage phenomenon of "initial rapid dehydration/de-ammoniation followed by stabilization" [21, 22]. In the low-temperature stage (approximately 20–200°C), the mass loss is primarily attributed to the evaporation of free/adsorbed water in pores and the dehydration of struvite (releasing H_2O), as described by Equation (4); this stage typically makes the dominant contribution to the total mass loss. In the medium-temperature stage (approximately 200–600°C), $MgNH_4PO_4{\cdot}6H_2O$ undergoes further dehydration and de-ammoniation decomposition to form $Mg_2P_2O_7$, releasing NH_3 and H_2O (Equation (5)), which corresponds to the rapid mass loss observed after exposure to temperatures in the range of 20–600°C. As the temperature

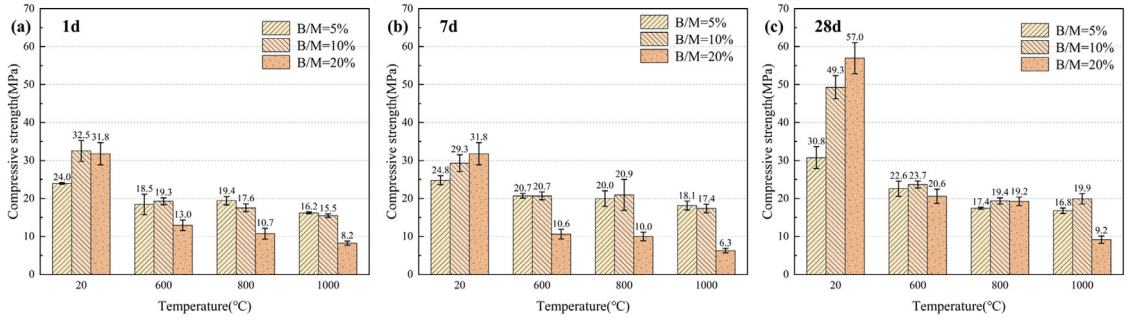

Figure 6 Effect of the B/M ratio on the compressive strength of MAPC pastes before and after high-temperature exposure (M/P = 3.0, W/C = 0.15, (a): 1 d, (b): 7 d, (c): 28 d)

increases into the 600–800°C range, $Mg_2P_2O_7$ reacts with residual MgO to form the more thermally stable $Mg_3(PO_4)_2$ (Equation (6)). As this process involves negligible gas generation, the increment of mass loss diminishes significantly and the mass tends to stabilize.

After exposure to temperatures in the range of 800–1000°C, the system is dominated by MgO and $Mg_3(PO_4)_2$. With no new volatile components generated, the mass loss tends to stabilize. The influence of boric acid is manifested in two aspects. On the one hand, boric acid or borates undergo multi-step dehydration during the heating process and ultimately transform into B_2O_3. This directly introduces additional water loss, thereby amplifying the overall mass loss. On the other hand, the complexation and retardation effects of boric acid alter the hydration and crystallization pathways. This facilitates the retention of a certain proportion of hydrous/ammonium-bearing hydration phases or intermediate phases at the same curing age, which release more H_2O and NH_3 upon heating, further increasing the total mass loss. In the later stage of high temperatures (≥600°C), the solid-state stabilization reaction (as shown in Equation (7)) may occur in the boron-containing system to form $Mg_3(BO_3)(PO_4)$. However, this process involves no gas generation and makes a limited contribution to the mass loss; it primarily alters the final crystalline phase composition and stability.

$$MgO + NH_4H_2PO_4 + 5H_2O = MgNH_4PO_4 \cdot 6H_2O \quad (3)$$

$$MgNH_4PO_4 \cdot 6H_2O = MgNH_4PO_4 \cdot H_2O + 5H_2O\uparrow \quad (4)$$

$$2MgNH_4PO_4 \cdot H_2O = Mg_2P_2O_7 + 2NH_3\uparrow + 3H_2O\uparrow \quad (5)$$

$$Mg_2P_2O_7 + MgO = Mg_3(PO4)_2 \quad (6)$$

$$Mg_3(PO4)_2 + B_2O_3 + 3MgO = 2Mg_3(BO_3)(PO_4) \quad (7)$$

$$2H_3BO_3 = B_2O_3 + 3H_2O\uparrow \quad (8)$$

Table 3 summarizes the theoretical mass loss of MAPC paste pastes after high-temperature exposure, calculated under the assumption that all reactions proceed to completion, neglecting any potential residual intermediate phases. For the MAPC paste with M/P = 3.0, W/C = 0.20, and B/M = 20%, the final mass loss is approximately 25.15%, which is consistent with the experimental result.

In Figure 7, the mass loss of MAPC pastes during heating exhibits a rapid increase between 20°C and 600°C, followed by a gradual increase from 600°C to 1000°C. This trend aligns with the theoretical analysis described in Equations (4)–(7). The mass loss of MAPC pastes after high-temperature exposure decreases with an increasing M/P ratio (1000°C: M/P = 1.5_29.1% vs. M/P = 3.0_26.6%). This phenomenon may be attributed to the relative deficiency of MgO at lower M/P ratios (1.5 and 2.0), which results in a slower hydration rate. Although the hydration reaction essentially concludes after final setting, the overall hydration progress is relatively retarded. Consequently, the

Table 3 **Theoretical mass loss of MAPC pastes after high-temperature exposure**

					Single-Step Mass Loss		Cumulative Mass Loss
					%	g/mol	%
Eq. (3) $MgO + NH_4H_2PO_4 + 5H_2O = MgNH_4PO_4 \cdot 6H_2O$ (20°C)							
	MgO	H_2O	$NH_4H_2PO_4$	$MgNH_4PO_4 \cdot 6H_2O$			
Molar Mass	40.3	18.0	115.0	245.3			
Initial Mass (g)	345.0	92.0	115.0	0.0	—	—	—
Residual Mass (g)	304.7	2.0	0.0	245.3			
Eq. (4) $MgNH_4PO_4 \cdot 6H_2O = MgNH_4PO_4 \cdot H_2O + 5H_2O\uparrow$ (105–200°C)					—	—	—
	$MgNH_4PO_4 \cdot 6H_2O$	$MgNH_4PO_4 \cdot H_2O$	H_2O				
Molar mass	245.3	155.3	18.0				
Initial mass (g)	245.3	0.0	2.0		13.93	92.0	13.93
Residual mass (g)	0.0	155.3	92.0				
Eq. (5) $2MgNH_4PO_4 \cdot H_2O = Mg_2P_2O_7 + 2NH_3\uparrow + 3H_2O\uparrow$ (200–600°C)							
	$MgNH_4PO_4 \cdot H_2O$	$Mg_2P_2O_7$	NH_3	H_2O	—	—	—
Molar mass	155.3	222.6	17.0	18.0			
Initial mass (g)	155.3	0.0	0.0	0.0	6.66	44.0	20.59
Residual mass (g)	0.0	111.3	17.0	27.0			
Eq. (8) $2H_3BO_3 = B_2O_3 + 3H_2O\uparrow$ (200–400°C)					—	—	—
	H_3BO_3	B_2O_3	H_2O				
Molar mass	61.8	69.6	18.0				
Initial mass (g)	69.0	0.0	0.0		4.56	30.1	25.15
Residual mass (g)	0.0	38.9	30.1				

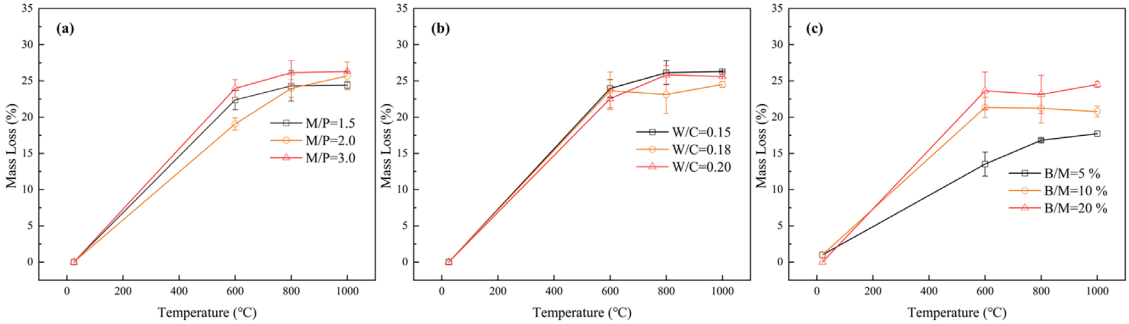

Figure 7 Mass loss of MAPC pastes after high-temperature exposure (28 d, (a): M/P, (b): W/C, (c): B/M)

final crystalline phases, such as struvite, are not fully developed. Instead, a certain proportion of hydration phases characterized by loose structure, high water content, and low thermal stability persists in the system. These components are prone to dehydration and decomposition at high temperatures, thereby resulting in a relatively higher mass loss.

The mass loss of the MAPC pastes after high-temperature exposure increases with an increasing W/C ratio, rising from 24.5% to 26.2% as the W/C ratio is raised from 0.15 to 0.20 (Figure 7b). This is attributed to the more complete hydration at higher W/C ratios, which generates a larger amount of hydration products dominated by struvite rich in crystallization water; notably, struvite is the primary source of mass loss.

Theoretical calculations indicate that the mass loss of MAPC reaches 25.15% at 600°C, beyond which no further mass loss is theoretically anticipated as no additional volatile sources emerge. However, experimental results demonstrate a continuous increase in mass loss with rising temperature: 23.96% at 600°C, 26.13% at 800°C, and 26.29% at 1000°C. The discrepancy at 600°C, where the theoretical value exceeds the experimental measurement, is attributed to the pre-volatilization of ammonia (NH_3) during the curing process, which reduces the available volatile content prior to calcination. The subsequent deviation observed from 800°C to 1000°C is primarily ascribed to the volatilization of boron trioxide (B_2O_3—derived from the decomposition of high-dosage boric acid—and the thermal decomposition of trace impurities present in the raw materials.

It is worth noting that the mass loss is most sensitive to the B/M ratio, followed by the W/C and M/P ratios. Specifically, at 28 d and 1000°C, the maximum mass loss differences for the M/P and W/C groups are only 1.9% (Figure 7a) and 1.8% (Figure 7b), respectively, whereas that for the B/M group reaches 6.8% (Figure 7c). This significant difference may be because the B/M ratio not only alters the reaction pathway and increases the proportion of decomposable phases but also because boric acid itself undergoes multi-step dehydration and transforms into B_2O_3 during heating, introducing additional mass loss and consequently leading to strength reduction (Figure 6).

3.4 Visual appearance

Figure 8 shows the visual appearance of the 28 d MAPC pastes before and after high-temperature exposure, demonstrating the influence of the B/M ratio after high-temperature exposure. It can be observed from Figure 7 that after high-temperature exposure, no cracks or spalling are visible on the

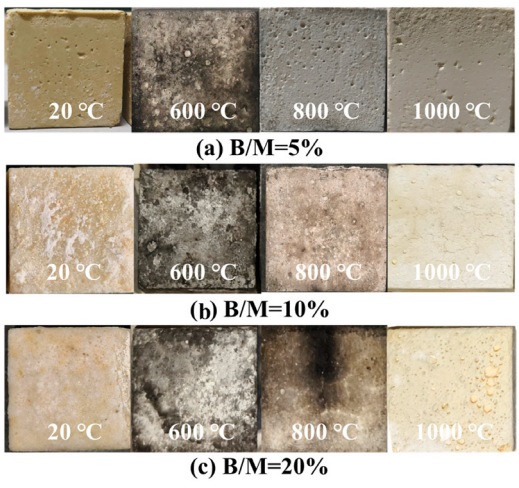

Figure 8 Visual appearance of MAPC pastes before and after high-temperature exposure (for 28 d)

Table 4 Effect of the M/P ratio on the porosity of MAPC pastes before and after high-temperature exposure

M/P	1 d				7 d				28 d			
	20°C	600°C	800°C	1000°C	20°C	600°C	800°C	1000°C	20°C	600°C	800°C	1000°C
1.5	2.40	37.70	44.82	47.49	2.70	36.79	43.42	45.79	2.57	37.73	41.06	42.80
2.0	1.03	38.28	42.17	47.31	2.17	36.71	41.38	47.44	1.01	38.36	40.05	47.69
3.0	1.43	35.82	35.43	39.74	1.77	33.63	34.81	39.10	1.86	36.26	35.17	41.38

Table 5 Effect of the W/C ratio on the porosity of MAPC pastes before and after high-temperature exposure

W/C	1 d				7 d				28 d			
	20°C	600°C	800°C	1000°C	20°C	600°C	800°C	1000°C	20°C	600°C	800°C	1000°C
0.15	1.47	29.32	31.08	31.78	1.12	27.96	30.61	29.75	1.63	27.76	28.68	30.20
0.18	1.53	31.96	33.46	37.68	1.62	30.48	32.81	36.56	1.00	33.17	33.39	37.88
0.20	1.43	35.82	35.42	39.74	1.77	33.63	34.81	39.10	1.86	36.26	35.17	41.38

surfaces of any pastes, and the structural integrity remains intact. With increasing exposure temperature, the surface color and state of all pastes exhibit a consistent evolution trend, undergoing a transition from earthy yellow/bright yellow (20°C) to dark gray/black (600°C), light gray (800°C), and finally light yellow/yellowish-white (1000°C).

3.5 Porosity

Table 4 shows the influence of the M/P ratio on the porosity of MAPC pastes before and after high-temperature exposure. The porosity decreases significantly with increasing M/P ratio, and the dominant role of M/P in determining the pore structure remains unchanged with increasing curing age. As shown in Table 4, at 1 d after exposure to 1000°C, the porosity values for M/P = 1.5, 2.0, and 3.0 are approximately 47.49%, 47.31%, and 39.74%, respectively. This phenomenon may be attributed to the higher content of unreacted MgO particles in the system at higher M/P ratios. During the hardening stage at 20°C temperature, these particles serve as fillers embedded within the skeletal structure formed by hydration products, effectively reducing the initial porosity and weakening pore connectivity. During high-temperature exposure, although dehydration decomposition of hydration products and structural shrinkage are inevitable, the "skeletal support" effect of residual MgO particles on the pore walls is more pronounced in high-M/P ratio systems. This effect can inhibit pore wall collapse and pore coarsening to some extent, thereby mitigating the increase in porosity [26]. This observation is consistent with the influence of the M/P ratio on the residual compressive strength after high-temperature exposure.

Table 5 shows the influence of the W/C ratio on the porosity of MAPC pastes before and after high-temperature exposure. The porosity increases significantly with an increasing W/C ratio (e.g., Table 5: at 7 d and 1000°C, W/C = 0.15 → 0.18 → 0.20, porosity = 29.75% → 36.56% → 39.10%). This may be attributed to the fact that a higher W/C ratio results in a higher content of residual free water after hardening, leading to the formation of more capillary and interconnected pores. Consequently, the pore diameter tends to coarsen, and the proportion of open pores rises, thereby increasing the porosity. During high-temperature exposure, these defective regions are more susceptible to dehydration, gas escape, and thermal stress concentration, inducing microcracks and pore interconnection, which further elevates the porosity. This observation is consistent with the influence of the W/C ratio on the residual compressive strength after high-temperature exposure.

Table 6 shows the influence of the B/M ratio on the porosity of MAPC pastes before high-temperature exposure. The MAPC pastes after high-temperature exposure exhibit low sensitivity to the B/M ratio. Only slight fluctuations are observed among different B/M ratios (a difference of 1.25% at 7 d and 1000°C), indicating that

Table 6 Effect of the B/M ratio on the porosity of MAPC pastes before and after high-temperature exposure

B/M	1 d				7 d				28 d			
	20°C	600°C	800°C	1000°C	20°C	600°C	800°C	1000°C	20°C	600°C	800°C	1000°C
5%	3.19	26.18	29.84	28.04	3.81	28.78	28.82	28.50	1.80	27.19	31.32	29.49
10%	1.70	25.98	29.77	30.11	0.99	24.31	29.57	28.63	1.64	29.84	31.08	31.54
20%	1.47	29.32	31.08	31.78	1.12	27.96	30.61	29.75	1.63	27.76	28.68	30.20

variations in boric acid dosage have a minor effect on the overall pore structure after exposure to temperature. Conversely, the porosity of MAPC pastes cured at 20°C temperature decreases with an increasing B/M ratio. This may be because a higher boric acid dosage prolongs the setting time, allowing the system to maintain higher fluidity for a longer period, which facilitates the formation of a relatively dense product network with fewer interconnected pores. However, the minor impact of the B/M ratio on porosity after high-temperature exposure likely accounts for the relative stability of the residual compressive strength observed across different B/M levels.

3.6 Mineralogical evolutions

Figure 9 shows the effects of M/P, W/C, and B/M ratios on the phase composition and content of MAPC paste after high-temperature exposure. It can be observed that with increasing exposure temperature, $MgNH_4PO_4·6H_2O$ transforms into $MgNH_4PO_4·H_2O$. After exposure to 800°C, distinct diffraction peaks of $Mg_3(PO_4)_2$ (PDF No. 33-0876) appear in the XRD pattern, indicating that the

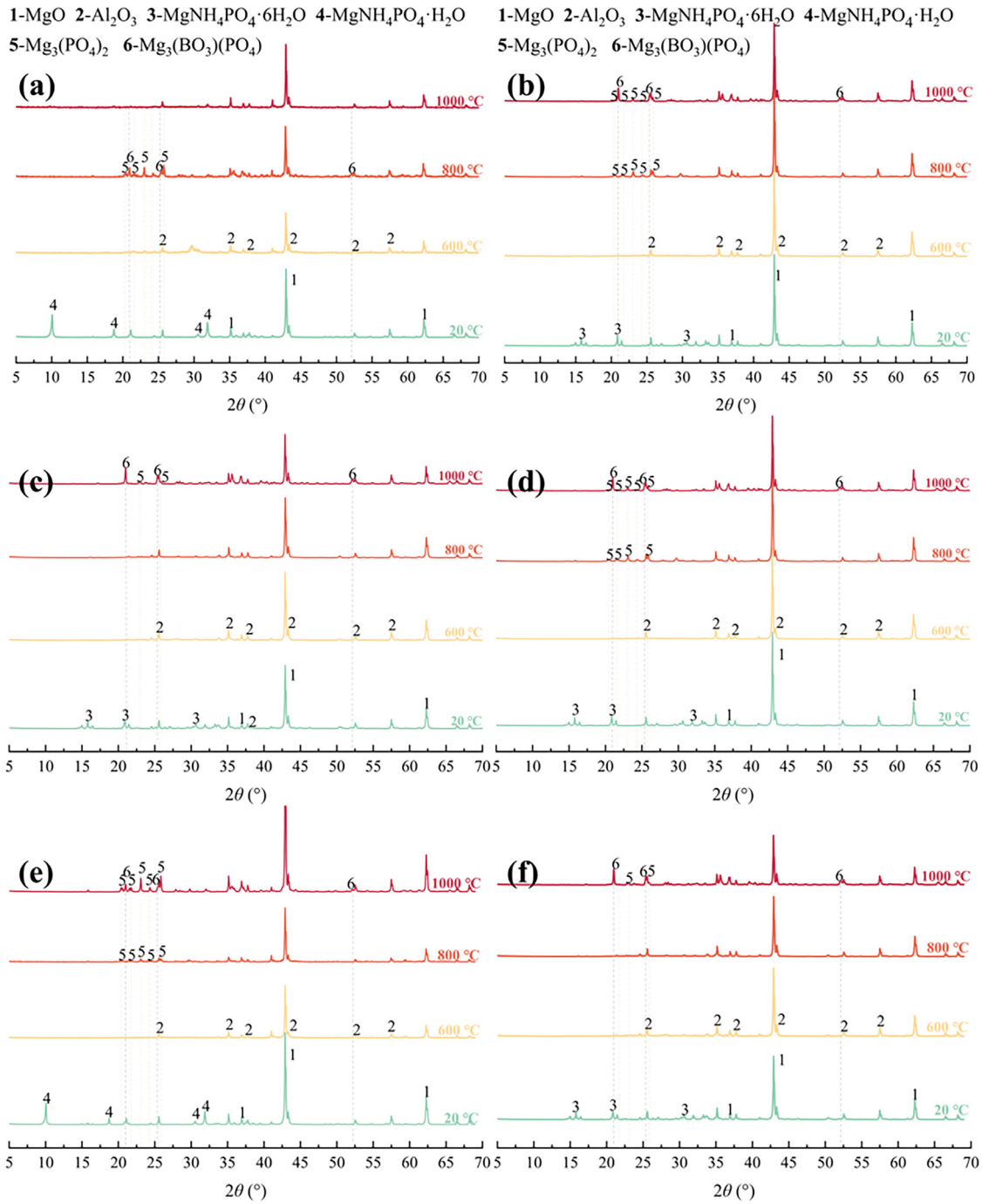

Figure 9 Phase composition of MAPC pastes before and after high-temperature exposure (for 28 d, (a): M/P = 1.5, (b): M/P = 3.0, (c): W/C = 0.15, (d): W/C = 0.20, (e): B/M = 5%, (f): B/M = 20%)

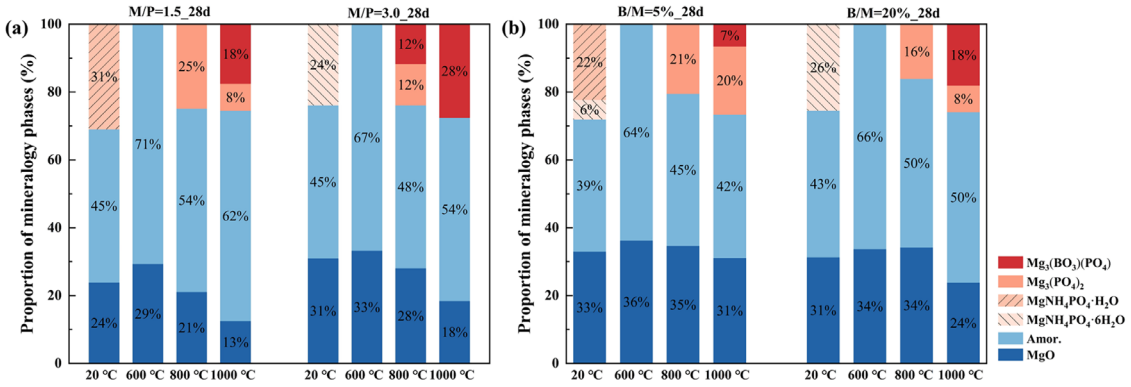

Figure 10 Quantitative phase composition of MAPC pastes before and after high-temperature exposure (for 28 d; (a): M/P ratio, (b): B/M ratio)

thermal decomposition of ammonium-bearing hydration phases is essentially complete. At 1000°C, $Mg_3(PO_4)_2$ reacts with the boric acid dehydration product B_2O_3 to form a new boron-containing phosphate phase, $Mg_3(BO_3)(PO_4)$ (PDF No. 53-0778), which is consistent with the results of the mass loss analysis.

The B/M ratio directly governs the formation extent of this new phase; a lower boric acid dosage results in less B_2O_3 available upon heating, thereby reducing the content of the new phase $Mg_3(BO_3)(PO_4)$ after exposure to temperatures. Increasing the M/P ratio significantly promotes the formation of $Mg_3(BO_3)(PO_4)$. As shown in Figure 10a, the content of the new phase $Mg_3(BO_3)(PO_4)$ after exposure to 1000°C increases from 18% to 28%. This may be attributed to the more sufficient residual MgO in the high-M/P ratio system, which provides a more favorable Mg source for the solid-state reaction between $Mg_3(PO_4)_2$ and B_2O_3 at high temperatures, thus driving the formation and accumulation of the new phase. Simultaneously, the residual MgO can participate in forming a more continuous load-bearing skeleton at high temperatures, supporting the residual strength. The W/C ratio has a minor effect on the content of the new phase $Mg_3(BO_3)(PO_4)$ after high-temperature exposure. The weak influence of the W/C ratio on the $Mg_3(BO_3)(PO_4)$ content indicates that the formation of this new phase is primarily controlled by the high-temperature solid-state reaction and the available M/B components, rather than being directly determined by the initial mixing water content.

The formation of $Mg_3(BO_3)(PO_4)$ may be detrimental to the maintenance of high-temperature residual strength. On the one hand, the formation of this phase is accompanied by boric acid dehydration and phase transformation, often corresponding to greater mass loss and pore development. Therefore, although the high-M/P system is more prone to generating $Mg_3(BO_3)(PO_4)$, the improvement in its residual strength is more likely attributed primarily to the supporting contribution of residual MgO.

It can be noted that the amorphous phase content in MAPC is relatively high after high-temperature exposure, which may be due to the higher boric acid content in the system. After exposure at 600°C, the phases of MAPC are mainly magnesium oxide and an amorphous phase, with almost no other phases present. This is possibly because the higher boric acid content in the system causes the decomposition products of struvite at 600°C to be predominantly in an amorphous form. $Mg_3(PO_4)_2$ has not yet formed, while $Mg_2P_2O_7$ is difficult to detect due to its low crystallinity.

3.7 Microstructural evolutions

Figures 11 and 12 show the influence of the B/M ratio on the phase morphology of MAPC pastes after exposure to 1000°C. It can be observed that the MAPC paste with B/M = 5% exhibits molten aggregates after high-temperature exposure (indicated by arrows in Figure 11a). EDS analysis reveals an Mg/P ratio of ≈3:2, identifying this phase as $Mg_3(PO_4)_2$, which exhibits an irregular morphology after water loss during high-temperature exposure. The MAPC paste with B/M = 20% (Figure 12) is primarily composed of plate-like crystal clusters stacked in a flower-bud-like structure after high-temperature exposure. EDS analysis shows an Mg/P ratio of ≈3:1, identifying this phase as $Mg_3(BO_3)(PO_4)$.

The residual strength of the matrix is primarily attributed to the continuous skeletal structure composed of MgO and $Mg_3(PO_4)_2$. At elevated boric acid dosages, the substantial generation of B_2O_3 during the dehydration process correlates with increased mass loss and potential pore coarsening. Furthermore, the chemical interaction between the generated B_2O_3 and the primary supporting skeleton ($MgO/Mg_3(PO_4)_2$) facilitates the formation of a new phase, $Mg_3(BO_3)(PO_4)$ (Equation (7)). This transformation potentially compromises the continuity of the initial framework, evolving into a microstructure characterized by the loose stacking of plate-like crystal clusters. Concurrently, the development of interfacial microcracks during cooling [43] may further impair the structural integrity, ultimately leading to a reduction in the overall load-bearing capacity and a decline in residual strength (Figure 6).

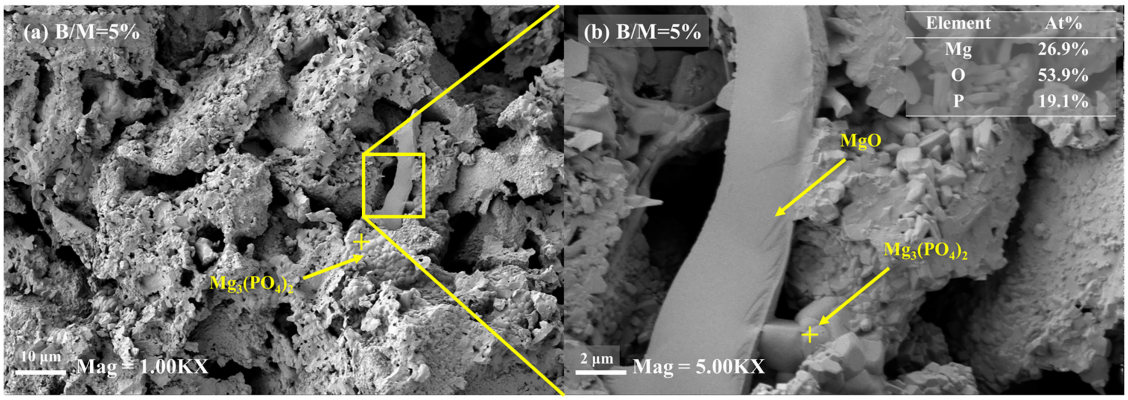

Figure 11 SEM of the MAPC paste (B/M = 5%, 28 d) after exposure to 1000°C ((a): mag = 1.00KX, (b): mag = 5.00KX)

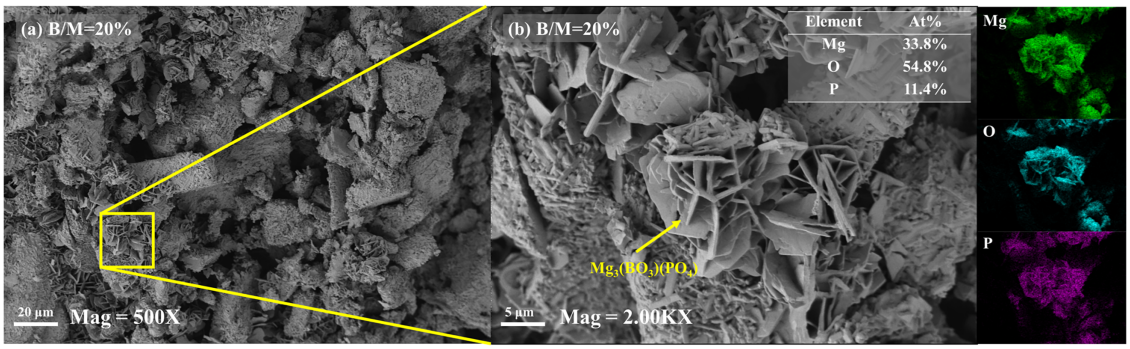

Figure 12 SEM of the MAPC paste (B/M = 20%, 28 d) after exposure to 1000°C ((a): mag = 500X, (b): mag = 2.00KX)

4 Conclusion

This study systematically investigated the influence of key mix parameters, the M/P, W/C, and B/M ratios on the high-temperature performance and degradation mechanisms of MAPC pastes. The primary findings are summarized as follows:

(1) An increasing M/P ratio accelerates setting and decreases fluidity. A higher W/C ratio retards setting and markedly increases fluidity. Boric acid primarily acts as a retarder, with only a marginal effect on fluidity.
(2) An increased M/P ratio enhances residual strength) by promoting the MgO-based framework. A lower W/C ratio improves residual strength by suppressing dehydration-induced damage and cracking via reducing free water and capillary porosity. Lowering the B/M ratio mitigates boric acid-induced thermal damage.
(3) The B/M ratio exerts the most pronounced influence on mass loss. This is primarily attributable to forming more decomposable phases and contributing directly to mass loss itself.
(4) After high-temperature exposure, porosity decreases with increasing M/P and increases with increasing W/C, while the B/M ratio has a minor impact.
(5) In systems with high boric acid content, boron oxide formed from the dehydration of boric acid reacts with the matrix to produce plate-like $Mg_3(BO_3)(PO_4)$ clusters. The disruption of the original structure is responsible for the observed strength deterioration.

Acknowledgement

We sincerely acknowledge all supervisors, colleagues and team members for their meticulous guidance, generous support and valuable suggestions throughout the research and manuscript preparation, to whom we pay our highest tribute. Meanwhile, this study was financially supported by relevant scientific research funds, for which we express our heartfelt gratitude.

Funding Statement

This work was supported by the Shandong High-speed Joint Fund (ZR2025LZN004), the Xinjiang 12th Division Science and Technology Plan Project (SRS2025209), and the Innovation Team Project of Jinan "20 New Rules for Universities in Jinan" Program (T202502).

Author Contributions

Yi Liu: Investigation, Formal analysis, Writing original draft. Jinguang Zhao: Formal analysis, Writing—original draft, Writing—review & editing. Pengkun Hou: Formal analysis, Writing—review & editing, Project administration, Funding acquisition. Hongsheng Wang: Formal analysis,

Writing—review & editing. Shuang Liang: Formal analysis, Writing—review & editing. Jie Hu: Formal analysis, Writing—review & editing. All authors reviewed and approved the final version of the manuscript.

Availability of Data and Materials

Data will be made available on request.

Ethics Approval

The authors declare that the data presented in this study are original and have not been fabricated or falsified.

Conflicts of Interest

The authors declare no conflicts of interest.

REFERENCES

[1] Fall M, Samb SS. Effect of high temperature on strength and microstructural properties of cemented paste backfill. Fire Saf J. 2009;44(4):642–51. doi:10.1016/j.firesaf.2008.12.004.
[2] Tu W, Fang G, Dong B, Zhang M. Multiscale study of microstructural evolution in alkali-activated fly ash-slag paste at elevated temperatures. Cem Concr Compos. 2023;143:105258. doi:10.1016/j.cemconcomp.2023.105258.
[3] You C. Hydration and hardening of magnesium phosphate cement and stability of hydration products [dissertation]. Chongqing, China: Chongqing University; 2017. (In Chinese).
[4] Liang M, Zhang Y, Xin X, Chen Z, Wang J, Jiao Y, et al. The properties of waterborne epoxy resins modified magnesium potassium phosphate cement paste: a combined experimental and molecular dynamics simulation study. Constr Build Mater. 2024;442(5):137494. doi:10.1016/j.conbuildmat.2024.137494.
[5] Ma C, Liu Y, Shi J, Zhang A, Song D, Zhou H, et al. Influencing mechanism of silica fume on early-age properties of magnesium phosphate cement-based coating for hydraulic structure. J Build Eng. 2022;54(10):104623. doi:10.1016/j.jobe.2022.104623.
[6] Zhao J, Shi J, Li Y, Hou P, Liang S, Chen H, et al. Phase and microstructure evolution of the hydration products of magnesium phosphate cements under sulfuric acid environments. Constr Build Mater. 2024;418(9):135465. doi:10.1016/j.conbuildmat.2024.135465.
[7] Shi J, Zhao J, Chen H, Hou P, Kawashima S, Qin J, et al. Sulfuric acid-resistance performances of magnesium phosphate cements: macro-properties, mineralogy and microstructure evolutions. Cem Concr Res. 2022;157:106830. doi:10.1016/j.cemconres.2022.106830.
[8] Liu X, Wang N, Zhang Y, Ma G. Optimization of printing precision and mechanical property for powder-based 3D printed magnesium phosphate cement using fly ash. Cem Concr Compos. 2024;148(4):105482. doi:10.1016/j.cemconcomp.2024.105482.
[9] Qin J, Zhang Z, Ma H, Dai X, Cheng X, Jia X, et al. Improving mechanical properties of magnesium phosphate cement-based ultra-high performance concrete by ultrafine fly ash incorporation. Constr Build Mater. 2024;448(3):138198. doi:10.1016/j.conbuildmat.2024.138198.
[10] Dong D, Huang Y, Pei Y, Zhang X, Cui N, Zhao P, et al. Effect of spherical silica fume and fly ash on the rheological property, fluidity, setting time, compressive strength, water resistance and drying shrinkage of magnesium ammonium phosphate cement. J Build Eng. 2023;63(3):105484. doi:10.1016/j.jobe.2022.105484.
[11] Zhang Z, Chang Z, Qian J, Hua Y, Wang A, Luo Z. Preparation and properties of sisal fiber reinforced magnesium phosphate cement. Compos B Eng. 2025;307(12):112859. doi:10.1016/j.compositesb.2025.112859.
[12] Yao P, Lin X, Wu Y, Ji T, Liang Y. Influence of slag on water resistance of magnesium silicon potassium phosphate cement. J Build Eng. 2024;97(1):110862. doi:10.1016/j.jobe.2024.110862.
[13] Liu F, Pan B, Zhou C, Nie J. Repair interface crack resistance mechanism: a case of magnesium phosphate cement overlay repair cement concrete pavement surface. Dev Built Environ. 2024;17:100355. doi:10.1016/j.dibe.2024.100355.
[14] Han H, Wang Z, Mosleh M. High performance basalt-fibre modified cement for elevated temperature environments. Constr Build Mater. 2024;448(13):138186. doi:10.1016/j.conbuildmat.2024.138186.
[15] Zhang A. Study on high temperature resistance modification of magnesium phosphate cement and in-plane shear between CFRP sheets and concrete [dissertation]. Harbin, China: Harbin Institute of Technology; 2017. (In Chinese).
[16] Dai X, Jia X, Qian J, Qin J. Preparation and properties of hydrotalcite-foamed magnesium phosphate cement for fire protection of steel structures. J Build Eng. 2023;76:107165. doi:10.1016/j.jobe.2023.107165.
[17] Dai X, Qian J, Qin J, Jia X, Tang H. Preparation and properties of gradient fire & corrosion protection magnesium phosphate cement coatings. Dev Built Environ. 2024;17:100327. doi:10.1016/j.dibe.2024.100327.
[18] Li Y, Wang N, Long S, Wang Z, Lin H, Mu J. Research on the properties of brucite-based magnesium phosphate cement fire resistive coating for steel structures. Constr Build Mater. 2024;449:138481. doi:10.1016/j.conbuildmat.2024.138481.
[19] Zhan Z, Sun W, Zhang S, Wen Q, Zhang H, Xiong X. Ablation resistance and mechanical properties of ZrB_2 reinforced magnesium phosphate cement composite. Constr Build Mater. 2023;364:129798. doi:10.1016/j.conbuildmat.2022.129798.
[20] Zhang S, Sun W, Zhan Z, Wen Q, Zhang H, Xiong X. Ablation and insulation properties of hybrid carbon-quartz fiber fabric reinforced magnesium phosphate cement composite. Constr Build Mater. 2025;464(13):140122. doi:10.1016/j.conbuildmat.2025.140122.
[21] Lv Y, Li T, Xu X, Yang J, Du Y, Hu X, et al. Effect of steel slag powder on the sulfate corrosion behaviour of magnesium potassium phosphate cement slurry. Constr Build Mater. 2024;456(1):139170. doi:10.1016/j.conbuildmat.2024.139170.
[22] Qiu H, Yu J, Chen H, Kuang D, He R. Investigation on a sustainable magnesium phosphate cement (MPC) with recycled waste MPC powders. J Environ Chem Eng. 2024;12(5):114160. doi:10.1016/j.jece.2024.114160.
[23] Bhuiyan MIH, Mavinic DS, Koch FA. Thermal decomposition of struvite and its phase transition. Chemosphere. 2008;70(8):1347–56. doi:10.1016/j.chemosphere.2007.09.056.
[24] Chau CK, Qiao F, Li Z. Microstructure of magnesium potassium phosphate cement. Constr Build Mater. 2011;25(6):2911–7. doi:10.1016/j.conbuildmat.2010.12.035.
[25] Hipedinger NE, Scian AN, Aglietti EF. Magnesia-ammonium phosphate-bonded cordierite refractory castables: phase evolution on heating and mechanical properties. Cem Concr Res. 2004;34(1):157–64. doi:10.1016/S0008-8846(03)00256-4.
[26] Sugama T, Kukacka LE. Magnesium monophosphate cements derived from diammonium phosphate solutions. Cem Concr Res. 1983;13(3):407–16. doi:10.1016/0008-8846(83)90041-8.
[27] Liu R, Wang W, Cui Y, Yang Y. Impact of metakaolin on hydration properties of magnesium phosphate cement. Case Stud Constr Mater. 2024;20:e02840. doi:10.1016/j.cscm.2023.e02840.
[28] Wang N, Bi W, Guo F, Guan Y, Li J. Effect of silica fume on the properties of magnesium ammonium phosphate cement at room temperature and high temperatures. J Mater Civ Eng. 2024;36(8):2065. doi:10.1061/JMCEE7.MTENG-17332.
[29] Qian W, Sun W, Li R, Wang J, Zhan S. Study on the high temperature performance of magnesium and potassium phosphate cement mixed with sucrose and its mechanism of action. Constr Build Mater. 2024;449(6):138523. doi:10.1016/j.conbuildmat.2024.138523.
[30] Liu Y, Chen Z, Ni H, Liu K, He J. High-temperature properties of fly ash and silica fume composite magnesium potassium phosphate cement. Constr Build Mater. 2024;441(6):137487. doi:10.1016/j.conbuildmat.2024.137487.
[31] Dai X, Zhang P, Gao Z, Qian J. Improving volume stability of magnesium phosphate cement at high temperatures by adding alumina-bearing admixtures. Constr Build Mater. 2025;487(8):142088. doi:10.1016/j.conbuildmat.2025.142088.
[32] Yu J, Qian J, Chen H, Ji Y, Kuang D, Jia X, et al. Behavior of magnesium phosphate cement with addition of sulphoaluminate cement at elevated temperatures. Constr Build Mater. 2023;401(6):132932. doi:10.1016/j.conbuildmat.2023.132932.
[33] Chen X, Guo J, Yu H, Zhang G, Kang Y, Zhang M, et al. Impact of calcination temperatures on lithium magnesium slag for enhanced magnesium phosphate cement properties. Constr Build Mater. 2024;451(3):138766. doi:10.1016/j.conbuildmat.2024.138766.
[34] Liu R, Wang W, Qi D, Yang Y. Static and dynamic mechanical properties of magnesium phosphate cement modified by metakaolin after high-temperature treatment. Constr Build Mater. 2023;392(4):131933. doi:10.1016/j.conbuildmat.2023.131933.
[35] Kwan YP, Alcock JR. The impact of water impregnation method on the accuracy of open porosity measurements. J Mater Sci. 2002;37(12):2557–61. doi:10.1023/A:1015460127828.
[36] Weng Y, Ruan S, Li M, Mo L, Unluer C, Tan MJ, et al. Feasibility study on sustainable magnesium potassium phosphate cement paste for 3D printing. Constr Build Mater. 2019;221:595–603. doi:10.1016/j.conbuildmat.2019.05.053.
[37] He Z, Zhu H, Shi J, Li J, Yuan Q, Ma C. Multi-scale characteristics of magnesium potassium phosphate cement modified by metakaolin. Ceram Int. 2022;48(9):12467–75. doi:10.1016/j.ceramint.2022.01.112.
[38] Xu C, Han J, Yang Y. A review on magnesium potassium phosphate cement: characterization methods. J Build Eng. 2024;82(7):108284. doi:10.1016/j.jobe.2023.108284.
[39] Xu B, Winnefeld F, Kaufmann J, Lothenbach B. Influence of magnesium-to-phosphate ratio and water-to-cement ratio on hydration and properties of magnesium potassium phosphate cements. Cem Concr Res. 2019;123:105781. doi:10.1016/j.cemconres.2019.105781.
[40] Hall DA, Stevens R, El-Jazairi B. The effect of retarders on the microstructure and mechanical properties of magnesia-phosphate cement mortar. Cem Concr Res. 2001;31(3):455–65. doi:10.1016/S0008-8846(00)00501-9.
[41] Xin Y, Sun W, Hu X, Wang X, Hou D, Xv F, et al. The effect of borax-urea composite retarder on the hydration process, microstructure and properties of magnesium phosphate cement. Constr Build Mater. 2025;493:143108. doi:10.1016/j.conbuildmat.2025.143108.
[42] Aghili S, Panjepour M, Meratian M. Kinetic analysis of formation of boron trioxide from thermal decomposition of boric acid under non-isothermal conditions. J Therm Anal Calorim. 2018;131(3):2443–55. doi:10.1007/s10973-017-6740-3.
[43] Gözel G, Baykal A, Kizilyalli M, Kniep R. Solid-state synthesis, X-ray powder investigation and IR study of α-Mg_3 [BPO7]. J Eur Ceram Soc. 1998;18(14):2241–6. doi:10.1016/S0955-2219(98)00152-6.